Environ. Chem. **2017**, *14*, 1–8
doi:10.1071/EN16070

Supplementary material

Heteroagglomeration of nanosilver with colloidal SiO_2 and clay

Sébastien Maillette,[A] *Caroline Peyrot*,[A] *Tapas Purkait*,[B] *Muhammad Iqbal*,[B] *Jonathan G. C. Veinot*[B] *and Kevin J. Wilkinson*[A,C]

[A]Biophysical Environmental Chemistry Group, Department of Chemistry, University of Montreal, CP 6128 Succursale Centre-ville, Montreal, QC H3C 3J7, Canada.

[B]Department of Chemistry, University of Alberta, Edmonton, AB T6G 2G2, Canada.

[C]Corresponding author. Email: kj.wilkinson@umontreal.ca

doi:10.1071/EN16070

Characterization of the colloidal suspensions

Particle size distributions were first measured for 100 mg L^{-1} of the colloidal suspensions (SiO_2, montmorillonite) in the absence of calcium at pH 7.0 (Figure S1). Simultaneous measurements of their diffusion coefficients (hydrodynamic size) and electrophoretic mobilities were performed at several calcium concentrations (Figure S2).

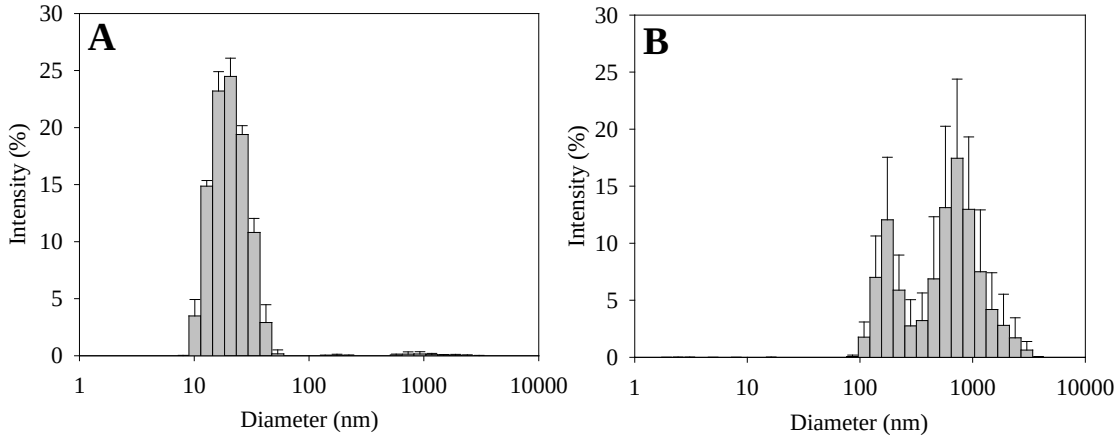

Figure S1. Particle size distributions (hydrodynamic diameters) obtained by dynamic light scattering for: (A) 100 mg L^{-1} of colloidal SiO_2 at pH 7.0 and (B) 100 mg L^{-1} of the colloidal clay particles (montmorillonite) at pH 7.0.

In Figure S1A, the size distribution obtained for colloidal SiO_2 showed a normal dispersion with a small portion of very large particles, whereas dynamic light scattering for the clay particles gave a bimodal dispersion at much larger particle sizes. At pH 7.0, both colloids were negatively charged across a wide range of Ca concentrations, although both colloids showed evidence for charge screening or Ca adsorption at the higher Ca concentrations (Figure 2, yellow squares). When the average diameters were plotted as a function of calcium concentrations, some agglomeration was observed at the higher ionic strengths for both of the colloidal particles (Figure S2, blue circles). For SiO_2, agglomeration primarily occurred for Ca concentrations of 35 mM and above (Figure S2A). Agglomeration of the clay particles started at much lower Ca concentrations of 0.1 mM and increased until the upper tested limit of Ca concentrations (10 mM; Figure S2B). The observed agglomeration of the montmorillonite, in spite of an overall negative EPM, can likely be attributed to interactions between the edge and surface sites [1]. The observed decrease in electrophoretic mobilities at higher Ca concentrations can likely be explained by the sedimentation of some of the larger particle agglomerates.

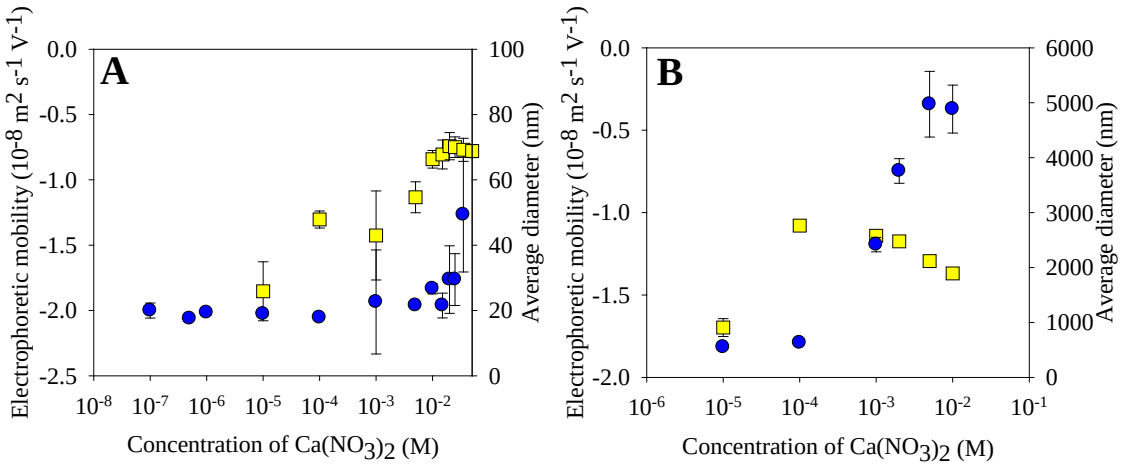

Figure S2. Hydrodynamic diameters (blue circles) and electrophoretic mobilities (yellow squares) as a function of added calcium concentrations for: (A) 100 mg L^{-1} of colloidal SiO_2 at pH 7.0; (B) 100 mg L^{-1} of colloidal montmorillonite at pH 7.0.

Labeling and characterization of the citrate stabilized nAg (nAg-cit)

Preparation of the nAg. Citrate stabilized Ag nanoparticles (nAg-cit) were either synthesized in house or purchased commercially. In the first case, nAg were synthesized from 10 mg of silver nitrate ($AgNO_3$, 99%, Aldrich), dissolved in 250 mL of deionized (DI) water (R>18 MΩ cm^{-1}) containing 9.0 mM citric acid (50 mg, 99%, Aldrich). Two drops of 4 M NaOH were added to the solution and it was heated to 70 ˚C for 1 h. The yellow/green solution that was formed was centrifuged in a 50 mL centrifuge tube at 12000 rpm (20000×g) for 30 min. A dark yellow/green precipitate was collected and redispersed in DI water to give the stock solution of nAg. The commercial citrate stabilized nAg (ca. 22 nm) were purchased from Nanocomposix (AGCB20) and used as received.

Synthesis of amine-terminated silver nanoparticles. Amine-terminated nAg were prepared by adding 100 μL of a 0.13 M aqueous cysteamine solution (cysteamine hydrochloride, 99%, Aldrich) in 10 μL increments to 25 mL of the nAg-cit dispersion (0.1 g L^{-1}). The solution was stirred overnight at room temperature and then centrifuged at 12000 rpm (20000×g) for 30 min prior to redispersion in 5 mL of DI water.

Conjugation of the rhodamine red-X with the NH_2-terminated nAg. Twenty-five mg of rhodamine red™-X, succinimidyl ester, 5-isomer (Life Technologies Inc.) was dissolved in 1.4 mL of dry DMSO. One mL of the aqueous NH_2-terminated nAg (above), 0.7 mL of

demineralized water and 7.5 mL of sodium tetraborate buffer (pH 8.5) were added to the rhodamine solution and the reaction mixture was stirred for 24 h at room temperature (see Figure S3). The reaction mixture was centrifuged at 12000 rpm (20000×g) for 30 min and particles were re-dispersed in DI water. A purified rhodamine labelled nAg was obtained after repeating the centrifugation step 3×. The labelled nAg-cit was dispersed in 5 mL DI water in order to obtain a final Ag concentration of 0.1 g L^{-1}.

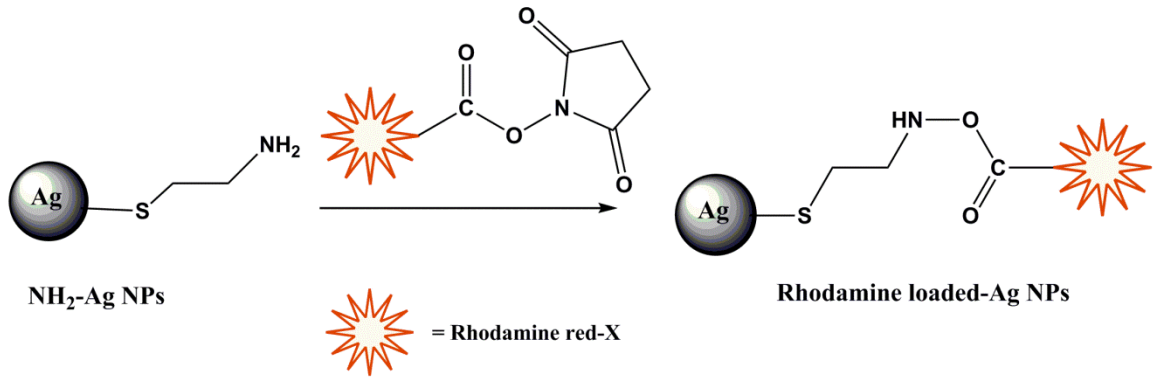

Figure S3. Synthesis of the rhodamine-labelled nAg-cit.

Characterization. Particles were characterized by transmission electron microscopy (TEM), UV-Vis absorption and photoluminescence (PL) emission spectroscopy, before and after the dye labelling. Samples were imaged with a JOEL 2011TEM with a LaB6 electron gun using an accelerating voltage of 200 kV. TEM samples were prepared by depositing a droplet of the aqueous suspension of nAg onto a carbon coated copper grid. UV-Vis absorption spectra and PL emission spectra of the nAg-cit and dye in dilute aqueous solutions were measured using a Carry 400 UV-Vis spectrometer and a Carry Eclipse spectrophotometer.

Following labelling of the homemade nAg-citrate, TEM images showed small nAg (Figure S4A) with an average diameter of 3.5 nm (Figure S4B). When the commercial nAg-cit was labelled, TEM images showed a monodisperse population of particles, with an average diameter of 21 ± 2 nm (Figure S5B,C) that were very similar to their initial sizes (Figure S5A). Nonetheless, there was some evidence for agglomeration (Figure 5B) and significant unbound fluorophore was found in the dissolved phase of the suspensions of the commercial particles. Particles were therefore extensively washed using a centrifugal ultrafiltration device (Amicon® Ultra-4 tubes, 3 kDa, Merck Millipore). The purification successfully removed excess fluorophore, but simultaneously reduced the average particle

sizes of the labelled nAg to 16 nm. All of the labelled nAg-cit had a significant negative charge on their surface, as demonstrated by their negative electrophoretic mobilities of -1.6 × 10^{-8} m^2 s^{-1} V^{-1} (in house 3 nm nAg-cit); -2.5 × 10^{-8} m^2 s^{-1} V^{-1} (commercial 21 nm nAg-cit) and -1.8 × 10^{-8} m^2 s^{-1} V^{-1} (commercial 16 nm nAg-cit following purification). The final covalently labelled nAg-cit that were used for the FCS experiments were fairly monodisperse suspensions of small particles (3 or 16 nm), containing no measurable unbound fluorophore.

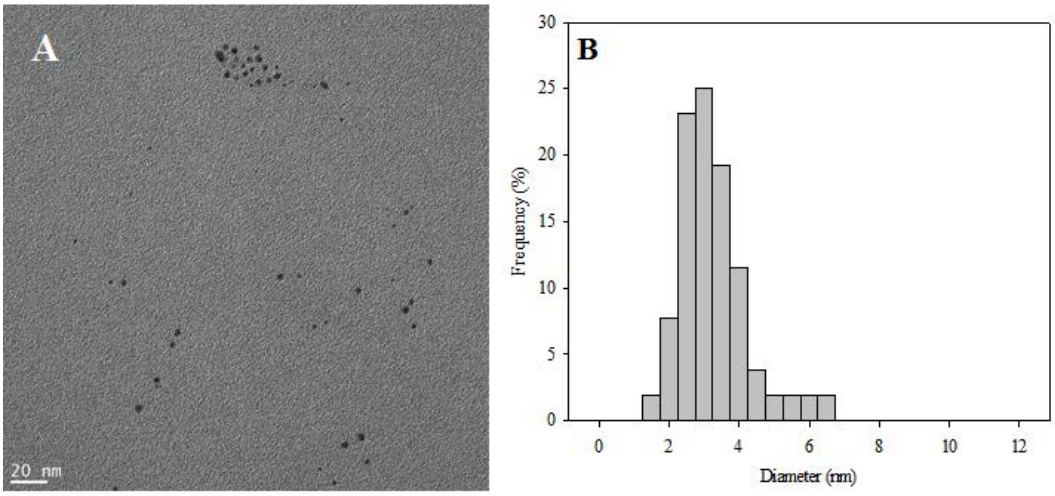

Figure S4. (A) TEM image of the citrate stabilized, rhodamine labelled nAg (homemade); (B) TEM distribution of the labelled nAg (N=55).

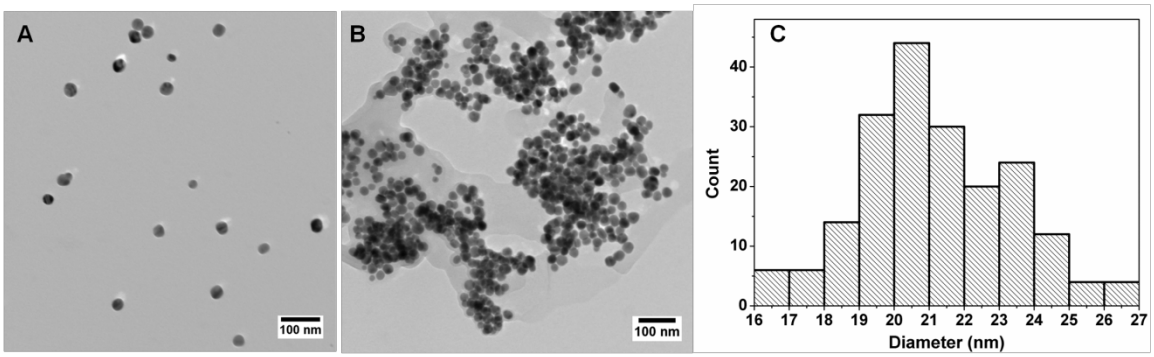

Figure S5. (A) TEM image of the commercial, citrate stabilized nAg, (B) TEM of the rhodamine labelled nAg-citrate; (C) TEM distribution of the labelled nAg-citrate (N=200).

doi:10.1071/EN16070

Labeling and characterization of nAg-PAA

Materials. Cross-linked, polyacrylic acid coated nanosilver (<10 nm) were purchased from Scivention (108SI). The size of the nanoparticle results, in large part, from the size of the polymer (ca. 100 kD) into which Ag is embedded. Quantification of the silver in the nanoparticles was performed using atomic absorption spectroscopy (Varian, Spectra A55). Sodium bicarbonate (>99.7%, Aldrich) was used to buffer the pH during the labeling process. Alexa Fluor® 488 NHS Ester (succinimidyl ester) was purchased from Invitrogen (A-20100) and used to label the carboxylic groups in the nanoparticle shell.

Conjugation of Alexa Fluor® 488 NHS ester with the nAg-PAA. Due to a low reaction efficiency, an excess of fluorescent dye (ca. 32 molecules of fluorescent dye per nAg) was used to label the carboxylated nanoparticles. Alexa Fluor® 488 NHS ester (succinimidyl ester, Mw = 643 g mol^{-1}) was added, with stirring, to a 2 g L^{-1} suspension of nAg in 0.1 M $NaHCO_3$ (pH 8.3). After 2 hours of mixing, excess reactive was removed by first passing the suspension over a desalting column (Figure S6, compare 'before' and 'after'). The remaining fluorescent dye was removed using centrifugal ultrafiltration (Amicon® Ultra-4 tubes, 3 kDa, Merck Millipore). Fluorescence in the filtrate decreased and became negligible after fifteen wash cycles. Silver was also quantified in the filtrate during the wash cycles with results showing that it was below quantification limits for graphite furnace atomic absorption spectrometry (ca. 0.5 µg L^{-1}). Indeed, the major Ag loss occurred during the initial wash on the desalting column and was at least partly associated with the adsorption/entrapment of particles by the column.

doi:10.1071/EN16070

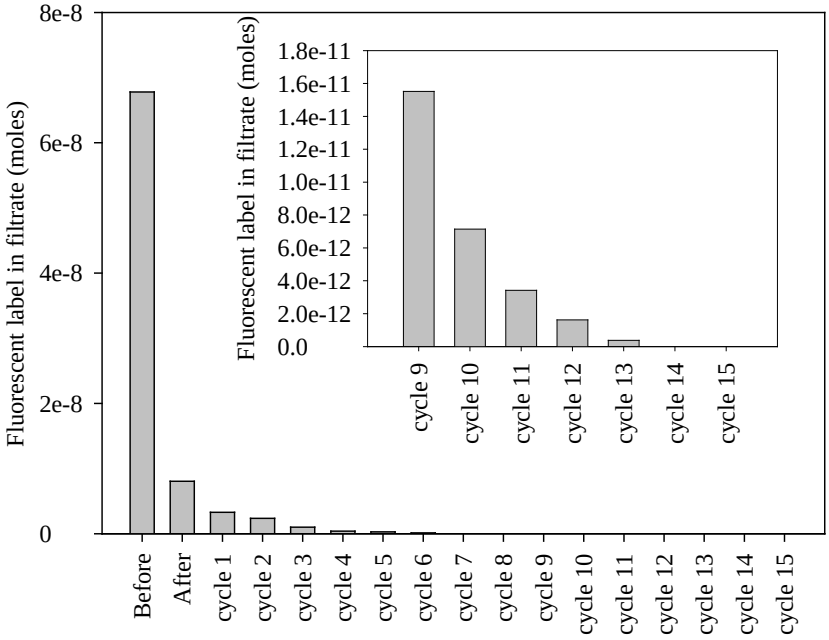

Figure S6. Efficiency of the washing of the labelled nAg suspension used to remove excess fluorescent dye. "Before" corresponds to the number of moles of label that were measured before the use of the desalting column while "After" corresponds to the number of moles that remained in solution after the use of the desalting column. Each of the remaining data points indicates subsequent cycles of centrifugal ultrafiltration.

Characterization. Size distributions of unlabelled and labelled nanosilver were determined using transmission electronic microscopy (TEM) and analytical ultracentrifugation (AUC). Average sizes of the nAg measured before and after the labeling process were similar (Figure S7). Electrophoretic mobilities were measured for unlabeled and labeled nAg. No significant changes in the EPM were observed due to the presence of the fluorescence dye on the particle surface (Figure S8) except at pH 4.0 (where no analysis was performed).

Of the two labelling techniques that were used, the labelling of the carboxylic acids on the particle stabilizer appeared to be the least perturbing, since the labelling and purification of the nAg-cit particles resulted in an apparent dissolution of the nAg. On the other hand, this direct labelling of the Ag surface is likely to be more applicable to a greater number of nAg particle types.

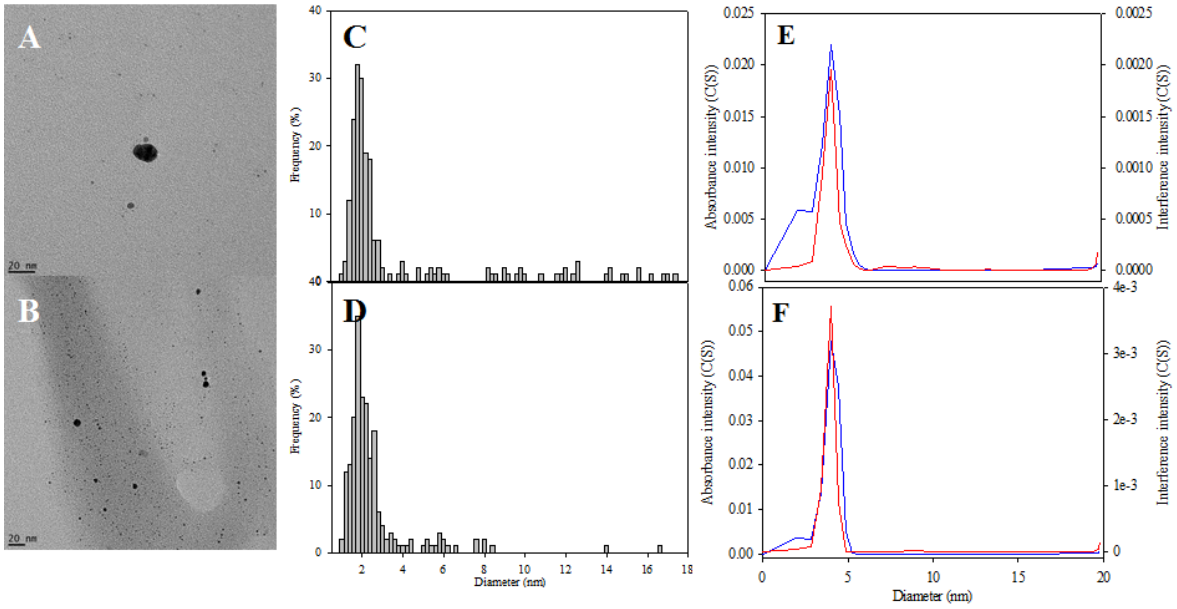

Figure S7. TEM and AUC on 5 mg L^{-1} of the nAg-PAA suspensions before and after labeling (A) TEM image of the nAg-PAA in Milli-Q water; (B) TEM image of the labelled nAg-PAA in Milli-Q water; (C) TEM size distribution of the unlabelled nAg-PAA (n=200); (D) TEM size distribution of the labelled nAg-PAA (n=200); (E) AUC distributions obtained using absorbance and interference detectors for the nAg-PAA in Milli-Q water and (F) AUC distributions using absorbance and interference detectors for the labelled nAg-PAA in Milli-Q water.

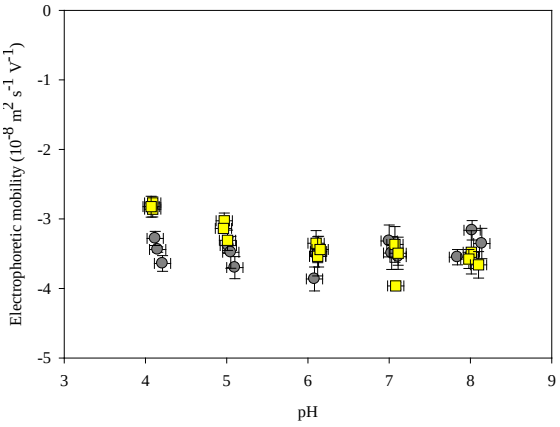

Figure S8. Electrophoretic mobility of unlabelled (grey circles) and labelled (yellow squares) nAg-PAA (5 mg L^{-1}) as a function of pH.

Fluorescence intensity measurements

Fluorescence intensity measurements in the confocal volume were also followed over time under the assumption that a loss in particles due to sedimentation would result in a decrease in fluorescence intensity. As anticipated, based upon the results obtained for the diffusion coefficients, fluorescence decreased with increasing Ca for the nAg-cit. In contrast, for the PAA stabilized nAg, fluorescence was constant across the entire range of measured Ca concentrations, reinforcing the observation that the nAg-PAA were extremely stable.

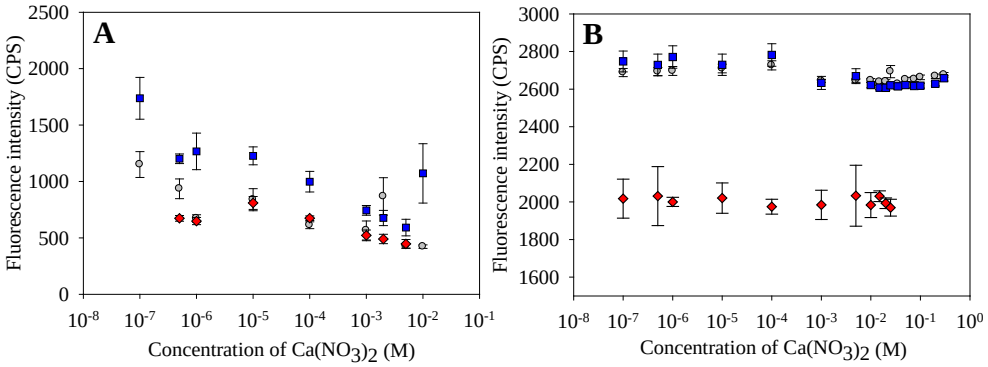

Figure S9. (A) Fluorescence intensity of labelled nAg-cit in the absence (grey circles) or presence of 100 mg L^{-1} of colloidal SiO_2 (blue squares) or colloidal clay (red diamonds) as function of added calcium at pH 7.0; (B) Fluorescence intensity of labelled nAg-PAA in the absence (grey circles) or presence of 100 mg L^{-1} of colloidal SiO_2 (blue squares) or colloidal clay (red diamonds) as a function of added calcium at pH 7.0 (the experiment with colloidal clay was performed independently; the overall decrease in fluorescence intensity was likely due to laser output).

Heteroagglomeration at pH 5

In addition to the heteroagglomeration experiments at pH 7.0 (Fig. 3), several experiments were also performed with the labelled nAg-PAA at pH 5.0 in the presence of the colloidal SiO_2. As seen above (Fig. S2), pH had a small effect on the electrophoretic mobilities of the nAg-PAA above pH 4.0. No homoagglomeration of the nAg was observed for added Ca ranging from 0.1 µM to 100 mM. Furthermore, addition of colloidal SiO_2 had no impact on the sizes of the nAg - PAA. The stability of the nAg was in sharp contrast with that of the colloidal SiO_2, which showed increased particle sizes, attributed to agglomeration, for Ca additions above 10 mM.

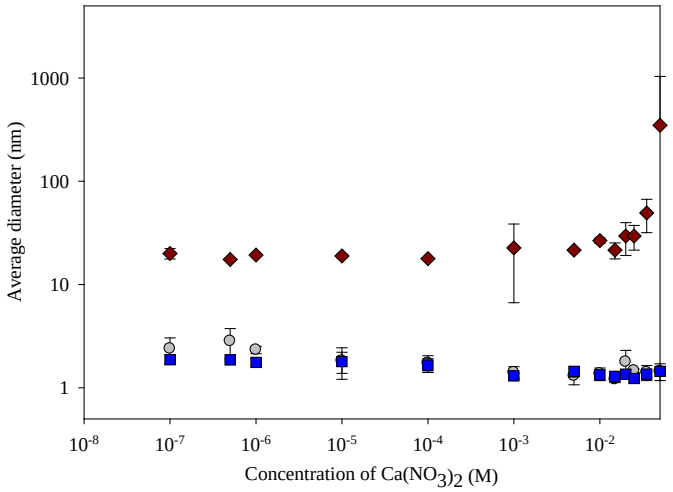

Figure S10. FCS determination of hydrodynamic diameters for 50 µg L^{-1} of nAg-PAA at pH 5.0, obtained over a large range of calcium concentrations: nAg-PAA only (grey circles); nAg-PAA in the presence of 100 mg L^{-1} of SiO_2 (blue squares). The brown diamonds show the measured agglomeration of SiO_2 alone, obtained using DLS.

Natural waters

Table S1. Characterization of the Des Prairies River water

TOC, total organic carbon

Component	Concentration
pH	6.5
TOC	6.9 ± 0.2 mg L^{-1}
Ca	20.8 ± 0.8 mg L^{-1}
K	1.73 ± 0.07 mg L^{-1}
Mg	6.0 ± 0.2 mg L^{-1}
Na	15.2 ± 0.7 mg L^{-1}

Enhanced dark-field microscopy with hyperspectral imaging

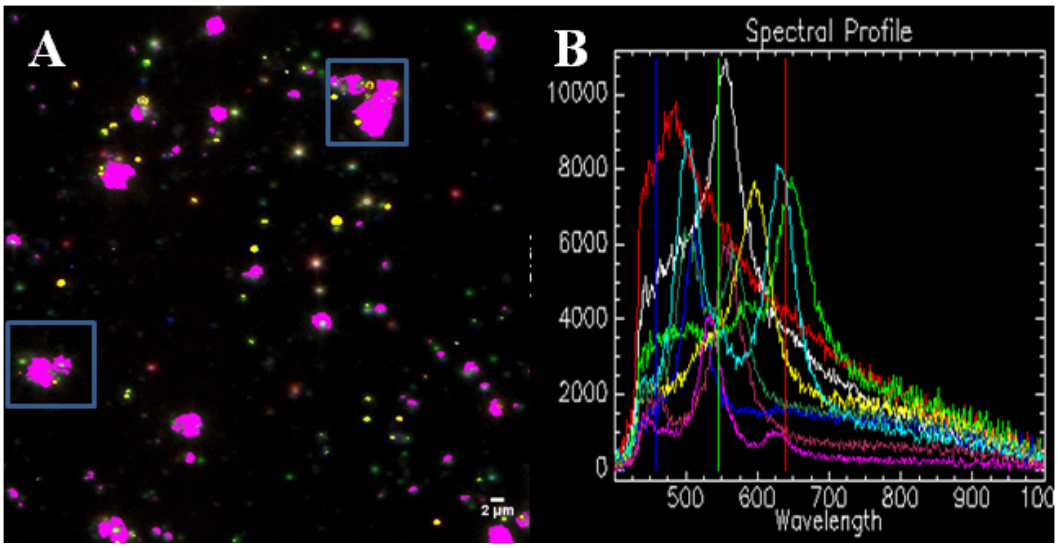

Figure S11. (A) Mapping of nAg-cit in presence of clay particles in 1 mM Ca at pH 7.0; (B) Spectral signatures of nAg-cit that were detected in the mixtures.

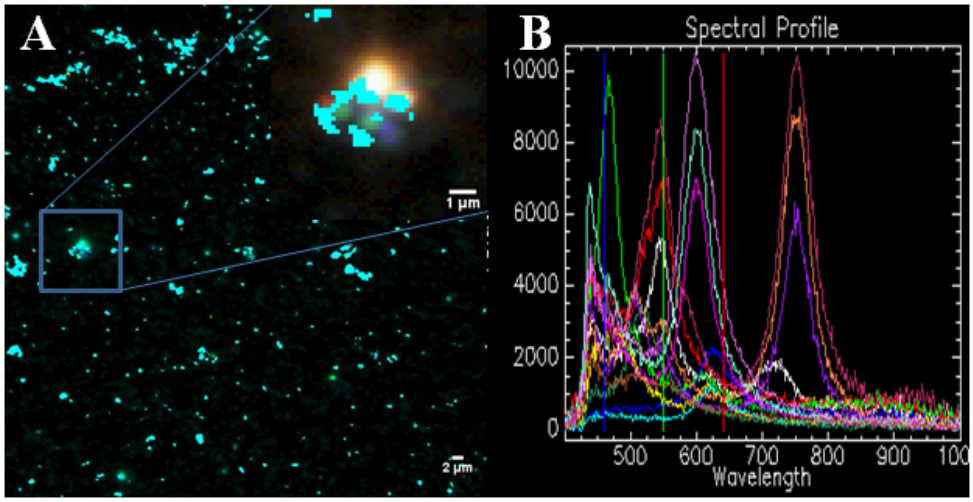

Figure S12. (A) Mapping of nAg-cit in presence of colloidal SiO_2 at 50 mM Ca; (B) Spectral signature of the nAg-cit that wasn't detected during nanoparticle mapping.

doi:10.1071/EN16070

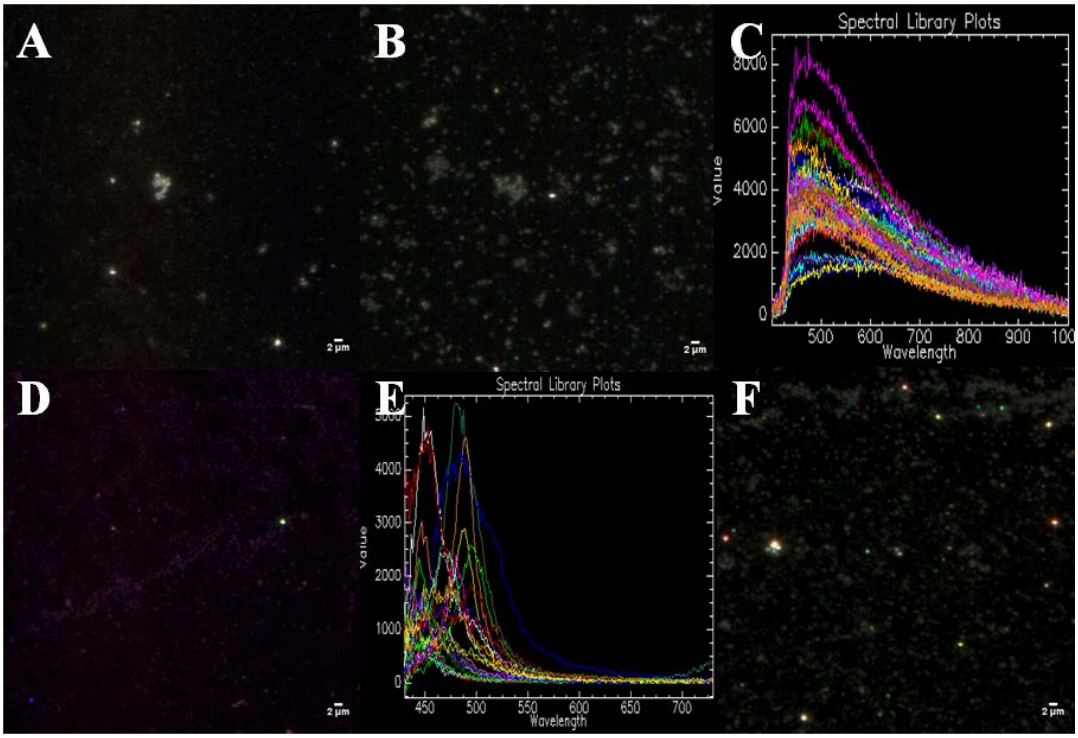

Figure S13. Darkfield microscopy and hyperspectral imaging analyses of the citrate coated nAg (22 nm) and the colloidal SiO_2: (A) 100 mg L^{-1} of colloidal SiO_2 in 1 mM Ca at pH 7.0; (B) 100 mg L^{-1} of colloidal SiO_2 in 50 mM of Ca at pH 7.0; (C) Spectral library for the SiO_2 generated from images similar to Figure 4A; (D) 1 mg L^{-1} of nAg and 100 mg L^{-1} of colloidal SiO_2 in 1 mM Ca at pH 7.0; (E) Spectral library of the nAg, generated in presence of the colloidal SiO_2; (F) 1 mg L^{-1} of nAg and 100 mg L^{-1} of colloidal SiO_2 in 50 mM Ca at pH 7.0.

Raw FCS data for the nAg-cit in the Des Prairies River

Based upon the data used for the autocorrelation function, it is clear that diffusion times for the nAg in the river water were dramatically shifted to the right (longer times), a result that is clearly indicative of larger particle sizes.

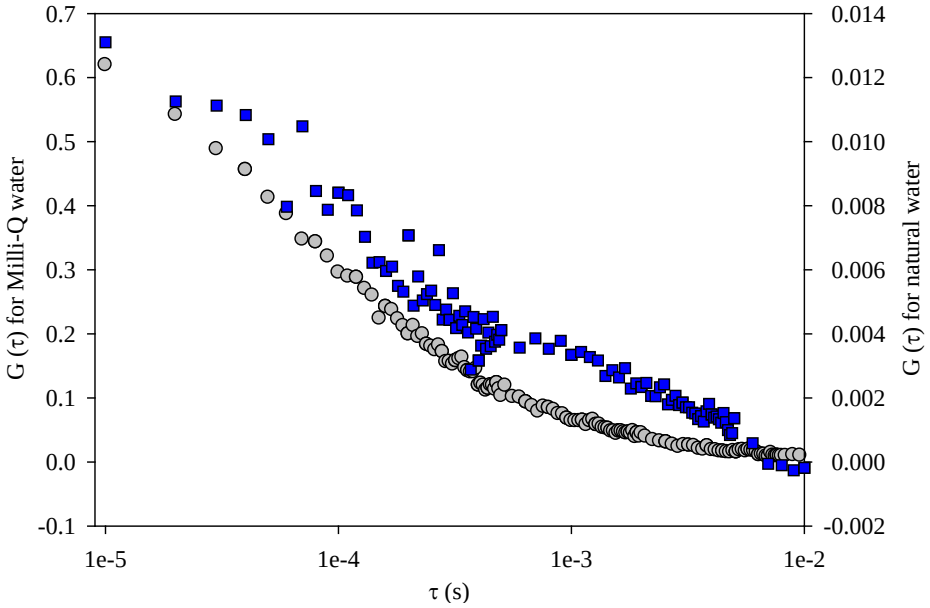

Figure S14. Autocorrelation curves obtained for 50 µg L^{-1} of rhodamine red-X labelled nAg-cit in Milli-Q water (grey dots) and in a 0.4 µm of a filtered water sample of the Des Prairies River (blue squares).

References

[1] R. A. Ruehrwein, D. W. Ward, Mechanism of clay aggregation by polyelectrolytes. *Soil Science* **1952**, *73*, 485.